ENHANCEMENT OF A MICROFLUIDIC DEVICE SEEDED WITH CELLS VIA CFD ANALYSIS

Elvira Darbayeva, B.Eng.

Submitted in fulfillment of the requirements
for the degree of Master of Science
in Mechanical & Aerospace Engineering

NAZARBAYEV UNIVERSITY

School of Engineering and Digital Sciences Department of Mechanical & Aerospace Engineering Nazarbayev University

53 Kabanbay Batyr Avenue,
Nur-Sultan city, Kazakhstan, 010000

Supervisor: Prof. Luis Rojas-Solórzano
Co-Supervisor: Dr. Gulsim Kulsharova

April 2022

DECLARATION

I hereby declare that this manuscript, entitled *"Enhancement of the microfluidic device seeded with cells via CFD analysis"* results from my work except for quotations and citations, which have been duly acknowledged.

I also declare that, to the best of my knowledge and belief, it has not been previously or concurrently submitted, in whole or in part, for any other degree or diploma at Nazarbayev University or any other national or international institution.

Name: Elvira Darbayeva

Date: April 2022

Abstract

Organ-on-a-chip technology can mimic the physiology of human organs and organ systems, help researchers better understand pharmaceutical drug effects on organisms before human clinical trials, and improve preclinical safety and efficacy of the drug testing. The key goal of this research is to use Computational Fluid Dynamics (CFD) techniques to evaluate the flooding properties of a microfluidic organ-on-a-chip device to enhance its functionality. The fundamental issue in the microfluidic chip design is the removal of entrained air bubbles that may remain after the fluid fills the chip, harming the cell observation process. This work aims to develop an enhanced microchip design utilizing CFD analysis to reduce entrained air while allowing proper residence time of the injected fluid and tolerable shear stress on the biological sample in the microfluidic chip. This thesis involved the creation of a CFD model on the ANSYS-CFX platform by discretizing the domain with the finite volume approach and solving the Navier–Stokes equations for air and water in the initial stage and water only in late-stage, in an Eulerian specification of the flow field.

Acknowledgments

First and foremost, I want to thank Professor Luis Rojas-Solórzano for his invaluable assistance, guidance, and encouragement. Throughout my Master's degree, his constant guidance was invaluable.

Second, I'd like to thank Professor Gulsim Kulsharova for her continuous support and direction throughout the research.

Elvira Darbayeva

Table of Contents

List of Tables

List of Figures

Chapter 1 - Introduction

Computational fluid dynamics (CFD) study fluid flow behavior in various domains and flow conditions [10]. CFD has many advantages over purely empirical analysis, including rapid simulation of coupled and complex designs at low cost and high robustness [7-10]. In particular, CFD has become very popular in the design optimization and analysis of microfluidic devices [1-6].

Several commercial and non-commercial open-source CFD codes have been developed over the years. Some of the most notorious CFD tools available for the global scientific and industrial community are CFD-ACE+, ANSYS-CFX/Fluent, FLOW-3D, OpenFoam, to mention a few. These software platforms can deal with complex fluid flows, including multi-component and multiphase fluid flows in their many different patterns [11-14].

The present investigation focuses on analyzing the flooding characteristics and enhancing the functionality of microfluidic devices for human tissue models for drug testing and disease modeling using ANSYS-CFX v19.2. The Navier-Stokes equations for the water and air interaction in the micro-chamber are discretized and solved in the Eulerian framework using the finite volume approach. The compressive high-resolution differencing scheme on the volume fractions convection is adopted to solve the free-surface and keep it sharp. The volume fraction computation adds up to 1 in every control volume [15-16]. The CFD tool solves the governing equations using a pressure–velocity couple technique, which demands more memory space than a traditional segregated method but allows for faster parallel processing convergence.

Organ-on-a-chip (OOC) is a micro-physiological device that can reduce the number of animal testing and the cost of drug testing (see Figure 1). OOC can replicate the functions of organs or organ systems so that the drugs can be tested before human clinical trials [17]. To create a robust OOC device, it is essential to provide successful growth of the cells and provide their stable functionality under continuous perfusion. Air bubbles worsen the cell observation process in flooded microfluidic chips during continuous perfusion [18]. As a result, this research aims to use CFD techniques to investigate the filling process of a microfluidic chamber to understand the variables that might reduce or remove air bubble capturing. The main goal of designing and enhancing the microfluidic device is the elimination of air bubbles left after the fluid filling process is complete and improve its effectiveness. Thus, using parametric analysis of the chamber area coupled with the CFD analysis, we plan to determine an improved chamber

shape that drastically reduces entrained air while allowing proper residence time of the injected fluid and minimizing the shear stress on the biological sample. The results of the analysis will be incorporated into the microfluidic device.

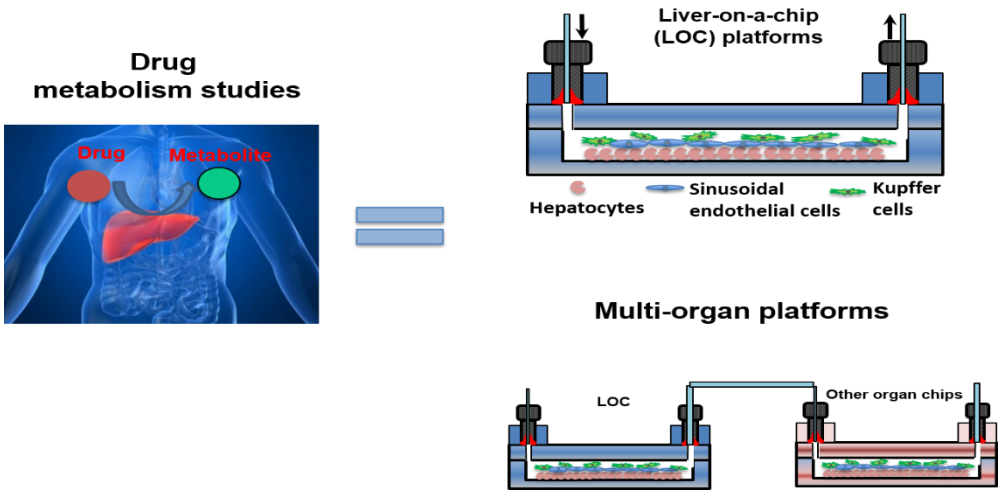

Figure 1. Organ-on-a-chip (Liver-on-a-chip) and Multi-organ platforms [19]

Chapter 2 - Methodology

2.1 Governing Equations and Physical Models

Water-air mass conservation and steady Reynolds-Averaged Navier-Stokes equations weighted by the volume fraction were prescribed as governing equations to be solved subject to the boundary conditions. It was assumed that each phase is an interpenetrating continuum, and every phase was supposed to exist in each position of the space, confined by friction, inertial, and gravity forces. The wall's capillarity was neglected because of the experimentally-verified contact angle of around 90° between the inner surface of the biosensor and the running fluids. A final equation was implemented to assure that the total volume of fractions in each control volume equals 1 as the summation of all phases [20].

Governing equations are determined by the following set of equations [15-16]:

Mass Conservation:

$$\nabla \bullet \left(r_a \rho_a U_a \right) = 0 . \qquad (1)$$

Momentum Conservation:

$$\frac{\partial}{\partial t}(\rho U) + \nabla \bullet \left(\left(\rho U \otimes U - \mu\left(\nabla U + (\nabla U)^T\right)\right)\right) = (B - \nabla p) \quad (2)$$

Thus, here,

$$U_\alpha = U_\beta = U \quad (3)$$

$$p_\alpha = p_\beta = p \quad (4)$$

$$\rho = \sum_{\alpha=1}^{2} r_\alpha \rho_\alpha \quad (5)$$

$$\mu = \sum_{\alpha=1}^{Np} r_\alpha \mu_\alpha \quad (6)$$

and, for the volume fractions,

$$\sum_{\alpha=1}^{2} r_\alpha = 1 \quad (7)$$

The upward buoyant force was prescribed in the z-axis because of the density differences between the phases, where U is the velocity field, p is the pressure field, ρ is the fluid density, μ is the fluid viscosity, and B is the body force (gravity only in this case) [15-16]. Constant properties of water and air at standard room temperature were considered in the analysis; consequently, consistent viscosity and density values were used [20].

Discretization of the computational domain into hexahedral(hex) and tetrahedral(tet) elements was performed. The finite volume method with an upwind differencing scheme in space and second-order backward Euler time-stepping was used to discretize the governing equations. The calculations were performed in the ANSYS-CFX v19.2 platform.

The chamber was initially filled with air, and then a series of numerical simulations were run with water running at 15 μl/min, 10 μl/min, and 5 μl/min flow rates. The outlet boundary condition was defined as 0 Pa and a zero velocity gradient. After a preliminary stability assessment, the t-step was set to 0.01 s, leading to a convergent and accurate solution within an acceptable computing time. The computer with the processor Intel(R) Core(TM) i5-1035G1 CPU and 8 Gb RAM memory was used in this study to simulate the fluid flow in the microchip. A simulation with the transient flow and uniform 0.01 t-steps was conducted to advance until the outlet tank was half-filled. The average simulation time was between 24-36 hours.

2.2 Computational Domain and Boundary Conditions

The CAD model of the organ-on-a-chip subject to this study was created using Solidworks. The assembly consisted of top and bottom parts and two fixators, as shown in Figure 2. After the geometry was exported to ANSYS DesignModeler, the outer faces were deleted to get the fluid-filled CAD domain. Because any simulation has memory and CPU time constraints, the geometry was divided by cutting through the plane of symmetry, and one side tube was removed, as illustrated in Figure 3A. The study region consisted of one micro-chamber and two micro-channels (see Figure 3B). The micro-chamber, in which air and water were expected to mix throughout the filling process, was located between two micro-channels. The micro-chamber and micro-channels, shown in Figure 3B, have the following dimensions: micro-channel width of 1mm, length of 13 mm, and height of 1mm; micro-chamber diameter of 10 mm and micro-chamber height of 1 mm.

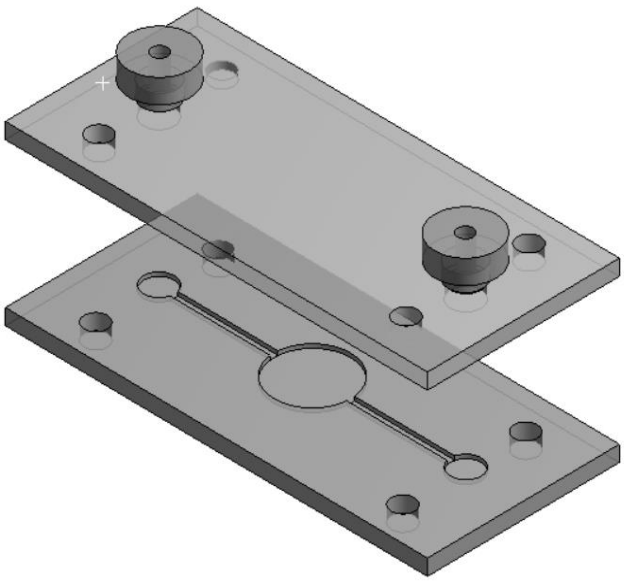

Figure 2. 3D CAD of "Organ-on-a-chip" [20]

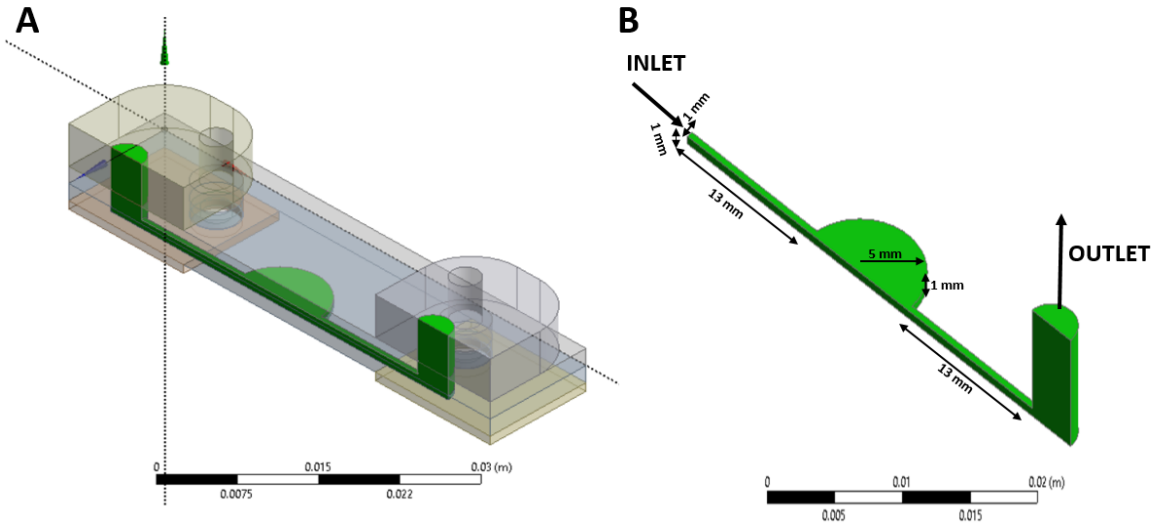

Figure 3. Computational domain (A) 3D view of the half computational domain (B) Default domain

Chapter 3 – Mesh Verification

Meshing or grid generation was performed before the simulation by discretizing the computational domain into nodes and elements. The mesh generation was done using the ANSYS Workbench Software with ANSYS Meshing. The computational domain was discretized into elements, and their nodes were located in the control volume centers (the vertices of the elements for ANSYS-CFX). The meshing was generated using tetrahedral, hexahedral, and prismatic elements. The mesh verification process was handled by performing a preliminary evaluation of mesh dependency with 83000 (Coarse), 166367 (Medium), and 332734 (Fine) elements. After a critical filling time is reached, the mesh sensitivity analysis compares the air volume fraction in the micro-channel and micro-chamber sections. The "critical time" (τ_c) is the estimated time required to fill the chip. The outlet tank located on the vertical connector section was not included in the calculation because of the need to estimate air entrapment through the micro-channels and micro-chamber only.

The bulk mass flow rate of 0.83×10^{-7} kg·s^{-1}, which equates to 5 µl/min, was used as the inlet boundary condition for the mesh sensitivity analysis. The pressure and velocity gradient were set to zero at the outlet boundary region. Figure 4 shows the flooding process, which

shows how the free surface evolves sequentially until the critical time (τc=330 s) is reached at the specified flow rate.

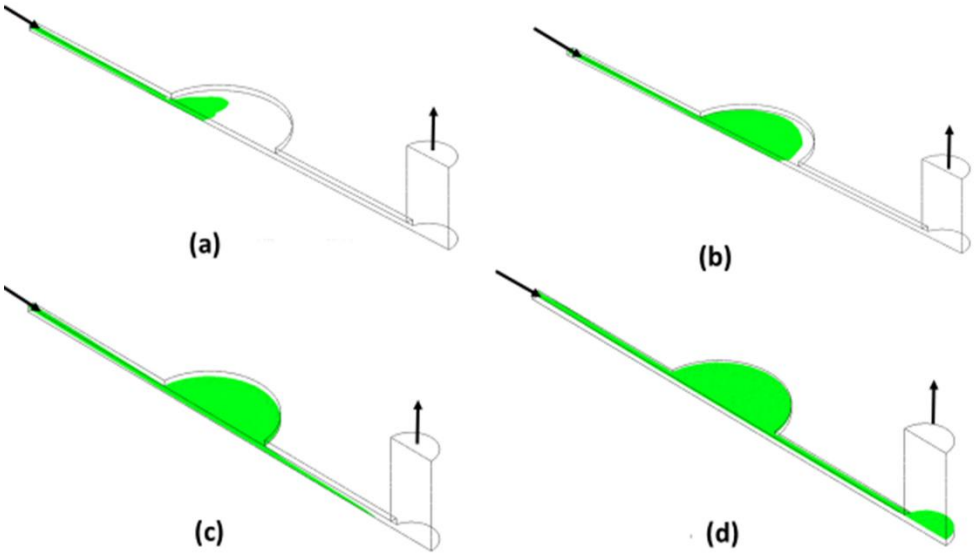

Figure 4. Free-surface during chamber flooding at an inlet liquid flow rate of 5 µl/min (a) 20s < τc; (b) 35s < τc; (c) 65 s < τc; (d) 330 s > τc [19]

After the chamber was flooded at a fixed time, the air volume fraction at the section was calculated and utilized to compare adjacent trial meshes. Table 1 shows the mesh verification findings and the variation between adjacent meshes. Then, a medium-sized mesh was chosen for the remained analysis.

Table 3.1. *Mesh sensitivity analysis [19]*

	Mesh-elements (Feature)	**Air Fraction**	**Deviation, %**
1	41000(XX-Coarse)	0.156	
2	83000 (Coarse)	0.187	16.6
3	166367 (Medium)	0.188	0.55
4	332734 (Fine)	0.188	0.16

Chapter 4 - Results and discussion

According to the initial numerical findings, under regular conditions for the original design, the microchip control region has 18.8% air entrapment.

It was observed that the flow was uniform and steady during the flooding. However, some waviness on the free surface, which might contribute to the air bubbles formation, was detected on the micro-chamber region.

The substantial air volume fraction, which equals 0.188 after the theoretical, critical time is reached, indicated that the filling process had failed to remove the air. For a flow rate of 10 µl/min, an overall air volume fraction of 0.245 showed a similar air behavior pattern at a critical time period. It proves that there is a directly proportional relationship between the inlet flow rate and air entrapped in the microchamber.

The model's height was decreased to 0.5 mm to minimize the entrapment of bubbles. After rerunning the CFD simulation, the resulting air volume fraction was 0.153, illustrating the excellent effect of lowering the chamber height. The level of unsteadiness of the free surface was discovered to be the most critical aspect in the air entrapment process, as the higher the chamber's height, the bigger the amplitude of the surface waves during the flooding process.

A new chamber configuration was considered in the study to facilitate the air release throughout the procedure. The numerical model was slightly inclined to the inlet direction to promote the migration of buoyant air bubbles towards the exit. After the critical period was reached, the simulation results showed a considerable drop in air-volume entrainment. The results showed 0.0032 and 0.0007 air volume fractions for 10° and 5° inclination, respectively. Similar results were obtained during the experiments with the inclined model, showing a positive effect of inclination during the validation process. The slight inclination of the model makes air trapping far more difficult to occur during the fluid filling process.

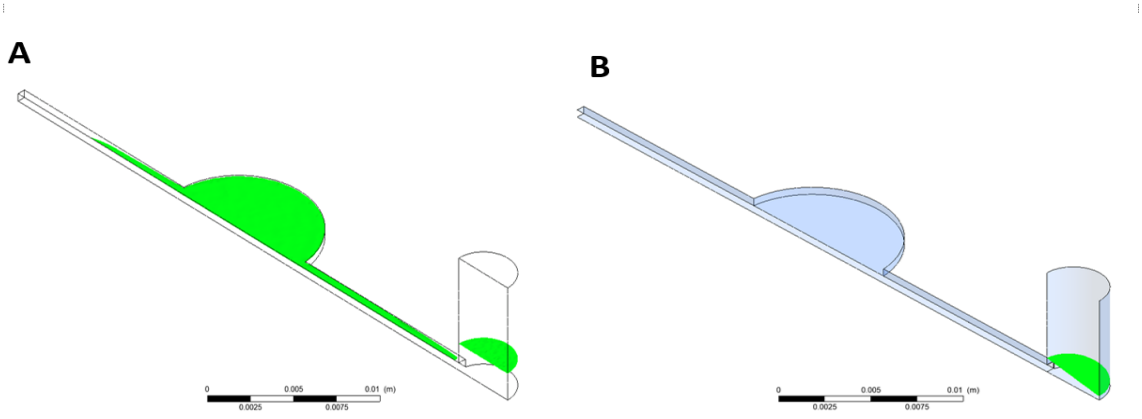

Figure 5. Free-surface during chamber flooding at an inlet liquid flow rate of 5 µL/min at critical time A) Reduced height to 0.5 mm B) Inclined surface for 10°

The CFD modeling results improved the HCP cell loading and washing procedures using a syringe, minimizing the air entrapment in the micro-chamber. The physical inclination of the device during filling processes for minor angles with a positive slope eliminated the entrainment of bubbles, verifying the CFD simulation results. The new inclined configuration was tested experimentally, positively affecting the cell loading and collagen coating processes.

A continuous fluid flow at a low rate did not demonstrate any bubbles entrapment in the micro-chamber during perfusion and wash-out procedures, allowing perfusion to be operated, after filling it, in a horizontal plane without any inclination.

Chapter 5 – Enhancement of the design

5.1. Role of oxygen in organ-on-a-chip devices

One of the essential factors in the hepatocytes microenvironment is oxygen, as it provides cellular metabolism, growth, and differentiation [21]; [22]; [23]. Coleman and Presnell (2003) claim that hepatocytes present a significant challenge in cell culture and probably "limiting cells" in vivo system due to their oxygen sensitivity [24]. In this study, the microchip was designed to culture human hepatocyte cell line Huh7 [19].

Microfluidic devices mainly use two types of oxygen transfer: perfusion and membrane aerated system [25].

In perfusion, oxygen is transferred using medium flow. However, the flow rate and oxygen solubility are limitations. In membrane aeration, the oxygen is delivered through the porous material, whereas imitations are material thickness and oxygen solubility [26], [27].

Tanaka et al. (2003) reported that oxygen and nutrients to the cell are supplied through perfusion [28]. According to Mehta and Korin, cells are exposed to different axial oxygen gradients within the chamber during the perfusion, and it has many consequences on the microenvironment [29],[30]. It is possible to overcome low oxygen values and decrease oxygen gradients near the walls by increasing the flow rate; however, it needs to be balanced with modest shear stress [25]. It was also observed that too high flow rates lead to waste of media and flushing out of cells from the chamber.

In the experimental work parallel to the present simulations, the microfluidic system was designed to combine perfusion and membrane aeration, as the upper layer of the model consists of porous polydimethylsiloxane (PDMS) material. The analysis in this investigation

assumes negligible oxygen delivery through the permeable PDMS layer, as the horizontal flow rate is much higher than vertical oxygen delivery through the pores. However, for simplification purposes, the CFD simulation in the present study will consider perfusion only, ignoring the membrane aeration through the upper PDMS layer.

According to Du et al. (2017), a fluid flow simulation is a key element to study the physiological microenvironment of the hepatic cells [31]. Rennert et al. (2015) conducted flow experiments to measure the impact of different medium flow rates on oxygen consumption of hepatic cells (from 1 µl/min to 10 µl/min) [32]. They identified that at 1 µl/min oxygen consumption is faster than oxygen supply and concluded that a minimum oxygen saturation happens at 3 µl/min.

The flow rate of 3 µl/min was used in the laboratory works parallel to this thesis, and it was visually estimated that the number of alive cells after 24 hours of perfusion was high (>90%). However, during the experiments, it was realized that cells were trapped near the walls of the chamber, and a significant number of dead cells were located near the peripheral walls. According to Lundhold et al. (2003), the edge zone is the main problem in microchips, and it may affect the results obtained from the microcell culture system [33]. The main objective of this section is to propose an optimal improved chamber shape design to enhance the effectiveness of the chamber, which will decrease the number of alive cells near the wall edges by balancing flow velocity and shear stress.

It was observed that the flow velocity is almost uniform over the center of the chamber, whereas the velocity varied widely between the center and edges. The flow velocity at the walls is 0 m/s (non-slip condition), and it starts to increase towards the symmetry line.

According to Mazzei et al. (2010), it is important to design microfluidic devices by maximizing mass transport between the cells [34]. Mazzei et al. (2010) designed a microchip which is called a MultiCompartmental modular bioreactor [34]. It consisted of cell-cultured (hepatocytes) microchamber and two microchannels. The chamber diameter was 12 mm, and different flow rates with different heights of the chamber were tested to identify the viability of the cells to the oxygen at different conditions. The authors reported that O2 concentration was always higher than the minimum threshold, even if the oxygen level fell rapidly at the walls' edge. Pedersen et al. (2016). presented velocity profiles for bioreactor developed by Mazzei et al. (2010), and they have reported that velocity ranges from 3*10^-6 m/s to 15*10^-6 m/s [35]. 3D simulations provided by the authors showed favorable results of shear stress level,

compound distribution, and above the critical level of oxygen concentration for hepatocytes. In this work, three μm/s will be used as the velocity threshold to supply sufficient oxygen for the hepatocyte cells.

5.2 Results of geometry enhancement: Velocity distribution

The axial velocity distribution over the centerline was analyzed and presented in Figure 6. Figure 7 shows the distance from the center versus the velocity chart. According to Figure 7, the velocity started from 0 at the walls and increased as expected towards the center. To estimate the level of enhancement, the area of effectiveness was used. An index of effectiveness is calculated by estimating the area of the chamber with velocity under minimum threshold values, subtracted from the overall area. The region under threshold velocity is estimated to be between 0 mm and 0.2 mm from the peripheral edge and the index of effectiveness, which is the area with sufficient velocity that guarantees the viability of cells, was estimated to be 92.15%. It was decided to design an oval-shaped chamber by reducing the X-axis radius and keeping the Y-axis radius of the original design. It was proved that decreasing the X-axis radius helps increase the velocity near the edge region, thus supplying sufficient oxygen to the cells near the walls. Figure 8 shows the distance from the center versus velocity distribution over the reduced radius, R=3 mm. It can be observed from Figure 9 that cells located between the wall and 0.05 mm from the wall would experience low velocity under the minimum required 3 mm/s. The effectiveness index for this particular shape was estimated to be 99.1%. Thus, it can be concluded that reducing the X-axis radius of the chamber from 5 mm to 3 mm, while keeping Z-axis radius the same, will increase the effectiveness of the chamber by 6.95%.

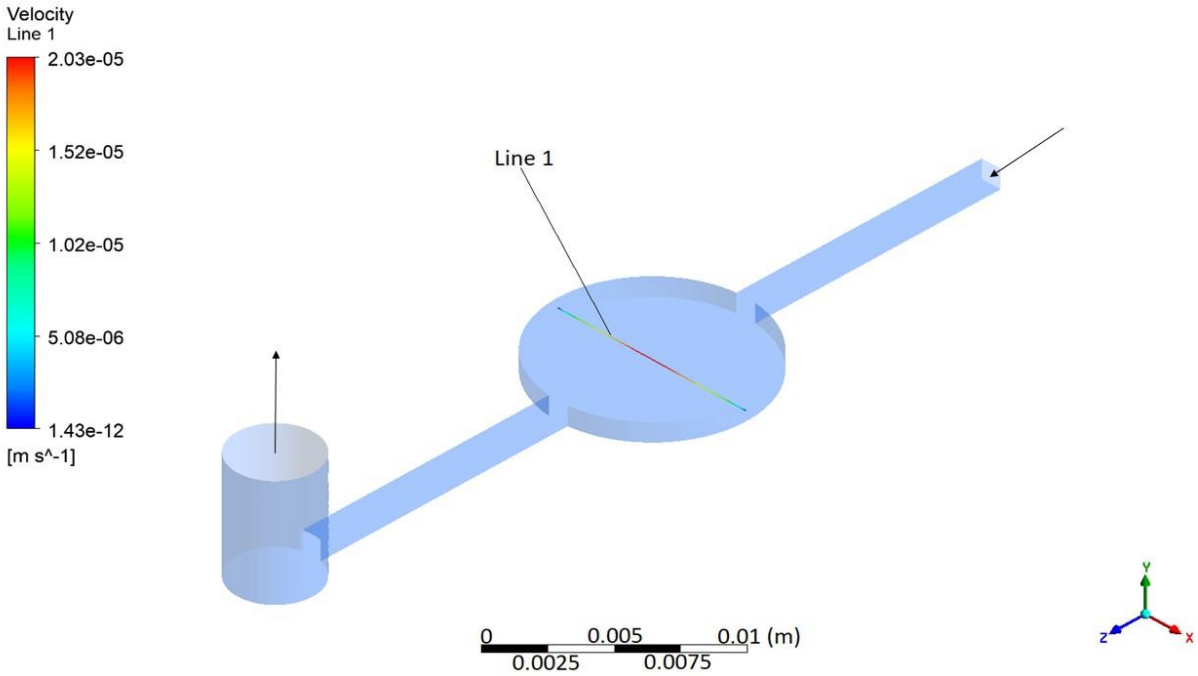

Figure 6. Streamwise Velocity distribution along @Line1

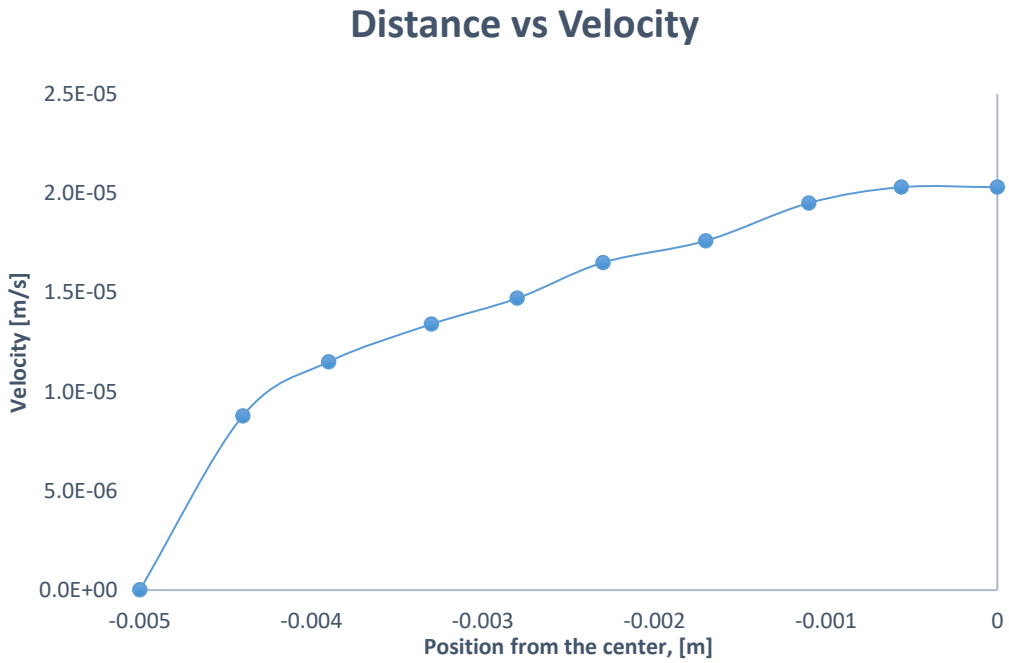

Figure 7. Velocity profile along @Line1 for circular design model

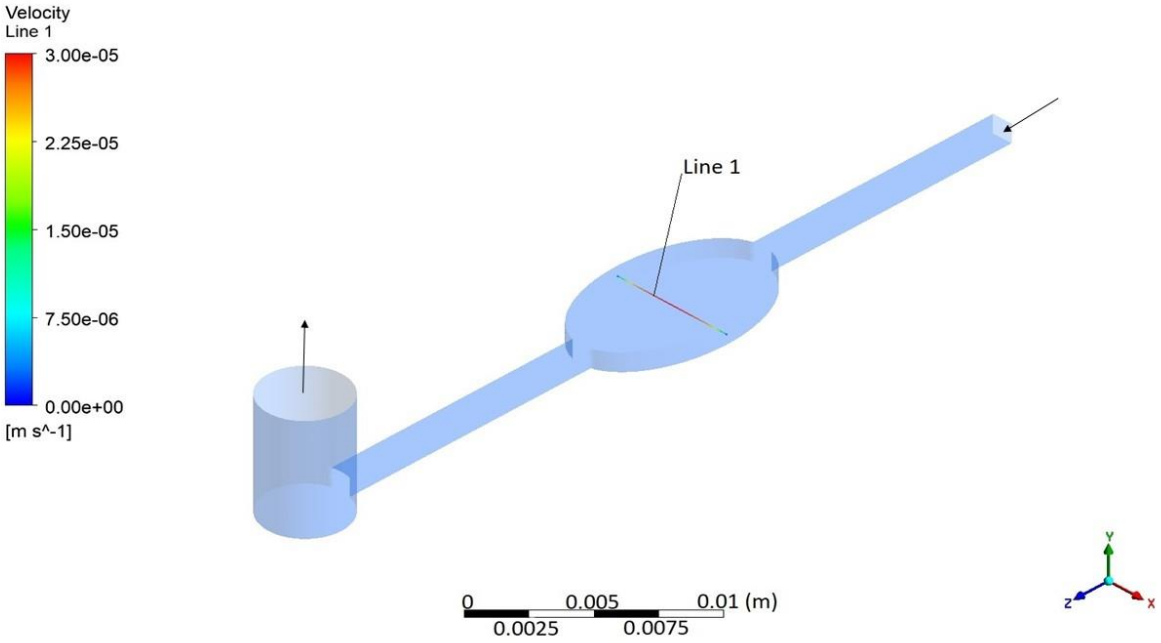

Figure 8. Streamwise Velocity distribution along @Line1

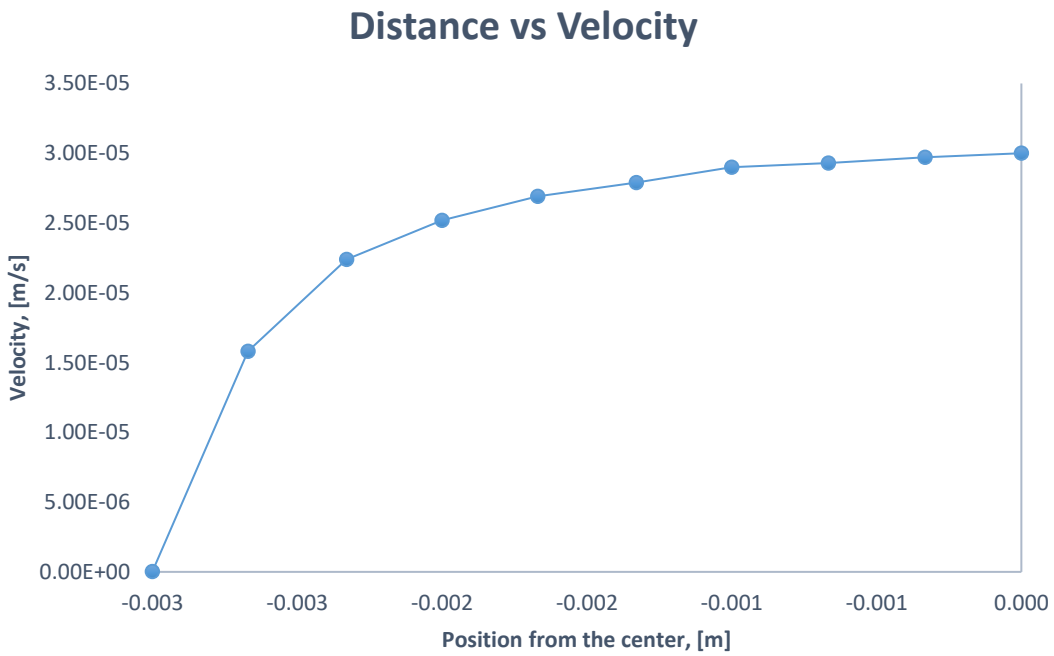

Figure 9. Velocity profile along @Line1 for elliptical design model

5.3. Role of Shear Stress in organ-on-a-chip devices

In microfluidic devices, mechanical forces have a major impact on cell behavior and functions. Fluid shear force is an example of the most common forces encountered by the microenvironment. The shear stress exists on any point of the fluid flow, but the shear stress on the walls is critical for this analysis as the cells are trapping near the walls.

Tanaka et al. (2006) reported that the hepatocytes changed their morphology and functions in response to the amount of shear stress they were exposed to [28]. Hepatocyte metabolic activity decreased under higher shear stress, especially when the cultivation time was longer than three days. Indeed, hepatocytes could be directly altered by blood flow under the perfusion. Thus, shear stress or other mechanical stresses are just as critical as nutrition and oxygen supply [12]. As a result, it is crucial to determine how the wall shear stress affects the hepatocytes' functions. The research studies suggest that exposing hepatocytes to relatively high pressure an be hazardous. Increasing the medium flow rate gives the cells more nutrients and oxygen, which also harms them. According to Goldstein et al. (2021), shear stress exposed to the cells strongly impacts cells' intrinsic physiology and hepatocyte's function, and their function is damaged at >5 dyn/cm2 (0.5 Pa) [36].

Du et al. (2017) mentioned that the fluid shear stress on the sinusoidal endothelium of the liver is estimated to be 0.1-0.05 Pa [31]. According to Delon et al. (2019), the physiologically relevant range for shear stress exposed by hepatocytes inside a single microfluidic device should be from 0 to 0.003 Pa [37]. Thus, threshold shear stress values of 0 (minimum) and 3 mPa (maximum) will be further used in this study to guarantee cell viability during the perfusion.

CFD simulation was performed to analyze shear stress on the bottom wall of the chamber.

5.4. Results of geometry enhancement: Wall Shear Stress

Wall shear stress has been used as a reference value of shear stress because it represents the maximum value of shear stress inside the microchamber [38].

Figure 10 shows the shear stress contour of the chamber with radius R=5 mm. The maximum shear stress value (1.422E-3 Pa) happened at the inlet, and chamber wall regions experienced the lowest shear stress. Even though shear stress at the center is approximately two times higher than in the edge region, the shear stress in overall chamber regions was under the maximum threshold value. It can be seen from Figures 10 and 11 that the highest wall shear

stress inside the chamber is experienced by the region of the inlet and outlet. Figure 12 shows the new design of the chamber, a more oval-shaped chamber with a radius decreased to 3 mm (R=3mm). Figure 13 shows the wall shear stress distribution inside the chamber. The minimum shear stress happens at the edges, and the maximum shear stress is located at the center. Overall wall shear distribution inside the chamber for 3 mm radius and oval-shaped design was under the threshold values of shear stress.

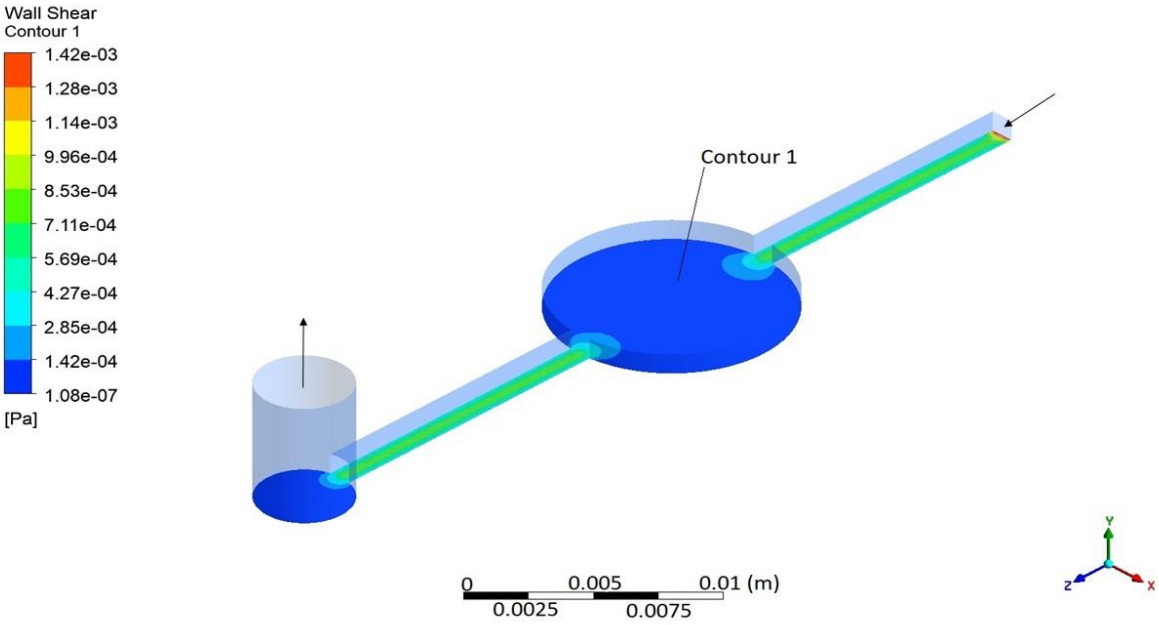

Figure 10. Wall shear distribution for the circular design model. Local range.

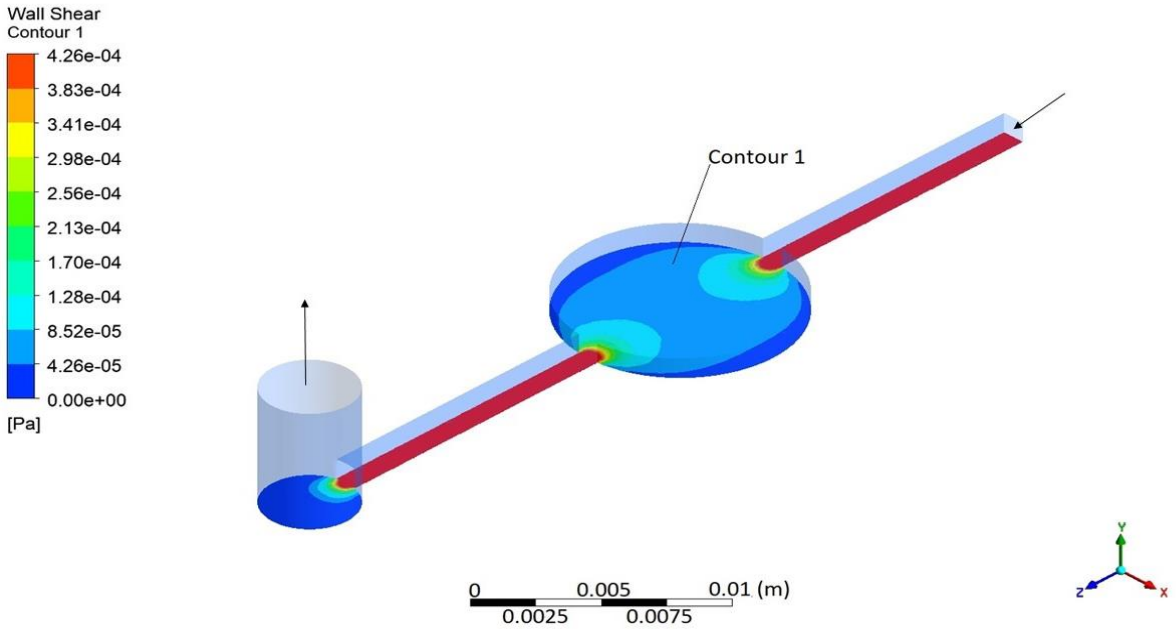

Figure 11. Wall shear distribution for the circular design model. User specified range.

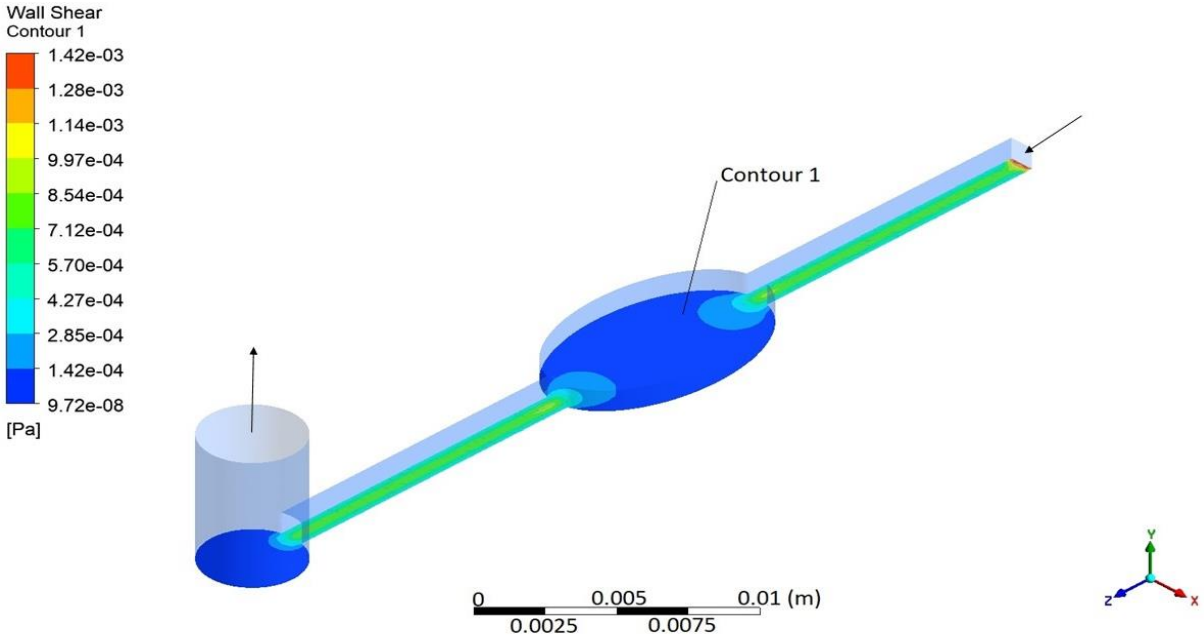

Figure 12. Wall shear distribution for the elliptical design model. Local range.

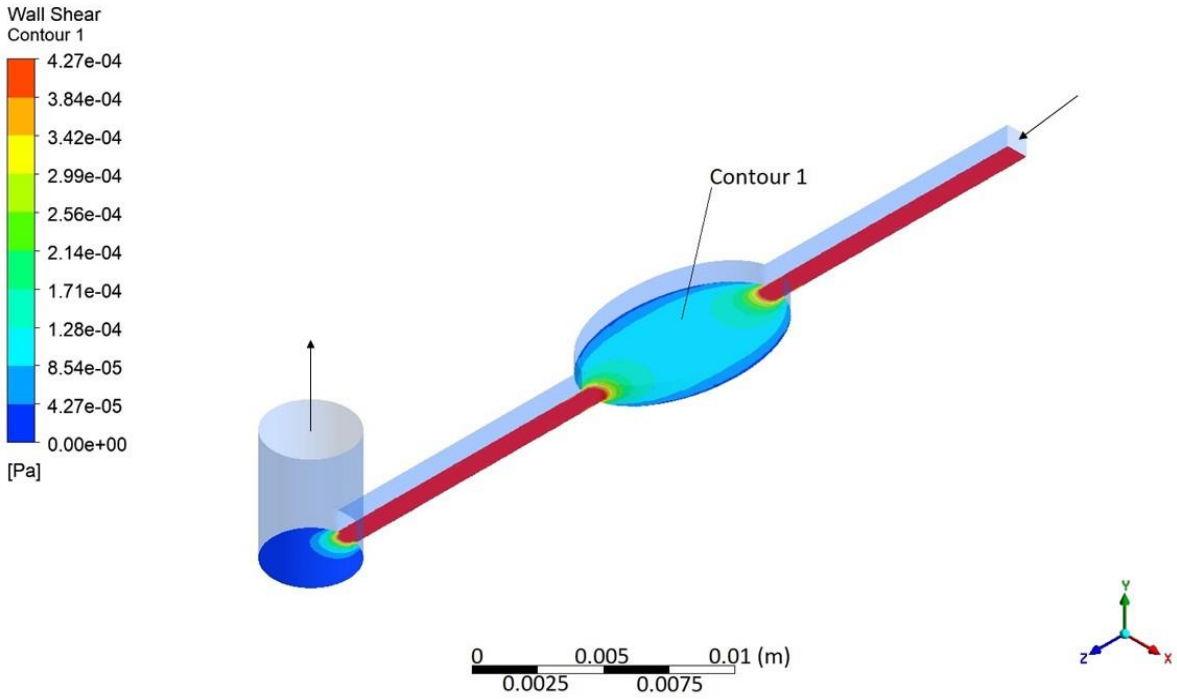

Figure 13. Wall shear distribution for elliptical design model. User specified.

Chapter 6. Limitations and future work

It was observed that most of the air particles were trapped near the wall of the micro-chamber, and its circular design complicates air exit to the micro-channel. The enhancement of the design section focused on investigating the influence of the micro-chamber shape change on air bubbles formation. The comparative study of the circular and more elliptic micro-chamber shapes performance was assessed using two output variables called residence time and shear stress at the bottom. Both of the parameters were selected to avoid cell extinction so that each cell will be nutriated enough time in the media and to assure that the flow will not wash away cells. However, there were limited time and setup restrictions for the enhancement process. There were some limitations to changing the shape and height of the chamber in the process of enhancement because the chip was intended to be placed on a microscope stand during its application. The porosity of the PDMS material was not included in the simulations, as it needed more time to conduct complex simulations combining both membrane aerated and perfusion systems.

Future work will mainly focus on conducting simulations with a membrane aerated system. For this purpose, bulk porosity of the PDMS and gas permeability of the air will be

included in the ANSYS CFX. Furthermore, different possible shapes of the chamber and their properties will be investigated for further use.

Chapter 7 – Conclusion

In this work, the formation of bubbles in the device and the process of the flow distribution were investigated using computational fluid dynamics simulations.

The presented results show that performing CFD simulation can help figure out air entrapment issues in microfluidic OOC devices by analyzing air volume fraction and parametric enhancement. It was shown that air entrapment in the micro-chamber constituted 18.8% initially, and a small decrease followed it to 15.3% after the height of the micro-chamber was halved. The same pattern was observed in the real validation assessment, showing smaller bubbles during the experiments run parallel to this investigation.

After that, the configuration with a slight inclination towards the inlet was suggested to ease the air entrapment. The numerical results showed a dramatic decrease in the air volume fraction entrapped and steady free surface.

In conclusion, the CFD study verifies that the micro-chamber height and model's angle of inclination can significantly affect the volume of air entrapment and the free-surface behavior.

The enhancement of the design was mainly focused on increasing the effectiveness by augmenting the area subject to flow speeds above a threshold within the micro-chamber. It was assumed that making a micro-chamber with an elliptic shape would help the air release process. The horizontal radius was decreased from 5mm of initial value to 3mm. According to the results the effectiveness was increased by approximately 7%.

References

[1] Zikanov, O. (2019). *Essential computational fluid dynamics*. John Wiley & Sons.

[2] Bhatti, M. M., Marin, M. I., Zeeshan, A., & Abdelsalam, S. I. (2020). recent trends in computational fluid dynamics. *Frontiers in Physics*, *8*, 453.

[3] Peng, S., Chen, Q., & Liu, E. (2020). The role of computational fluid dynamics tools on investigation of pathogen transmission: Prevention and control. *Science of The Total Environment*, 142090.

[4] Kim, K. Y., Samad, A., & Benini, E. (2019). *Design Optimization of Fluid Machinery: Applying Computational Fluid Dynamics and Numerical Optimization*. John Wiley & Sons.

[5] da Silva Júnior, J. L. (2019). An introduction to computational fluid dynamics and its application in microfluidics. In *Process Analysis, Design, and Intensification in Microfluidics and Chemical Engineering* (pp. 50-78). IGI Global.

[6] Ranjan, P. (2019). Investigations on the flow behaviour in microfluidic device due to surface roughness: a computational fluid dynamics simulation. *Microsystem Technologies*, *25*(10), 3779-3789.

[7] Shen, R., Jiao, Z., Parker, T., Sun, Y., & Wang, Q. (2020). Recent application of Computational Fluid Dynamics (CFD) in process safety and loss prevention: A review. *Journal of Loss Prevention in the Process Industries*, 104252.

[8] Kim, K. Y., Samad, A., & Benini, E. (2019). *Design Optimization of Fluid Machinery: Applying Computational Fluid Dynamics and Numerical Optimization*. John Wiley & Sons.

[9] Chaudhry, Q. A., & Al-Mdallal, Q. M. (2019). Review of design optimization of fluid machinery: applying computational fluid dynamics and numerical optimization.

[10] Shen, F., Li, X., & Li, P. C. (2014). Study of flow behaviors on single-cell manipulation and shear stress reduction in microfluidic chips using computational fluid dynamics simulations. *Biomicrofluidics*, *8*(1), 014109.

[11] Glatzel, T., Litterst, C., Cupelli, C., Lindemann, T., Moosmann, C., Niekrawietz, R., ... & Koltay, P. (2008). Computational fluid dynamics (CFD) software tools for microfluidic applications–A case study. *Computers & Fluids*, *37*(3), 218-235.

[12] Santana, H. S., da Silva, A. G., Lopes, M. G., Rodrigues, A. C., Taranto, O. P., & Silva Jr, J. L. (2020). Computational methodology for the development of microdevices and microreactors with ANSYS CFX. *MethodsX*, *7*, 100765.

[13] Lee, G. H., & Bae, J. H. (2019). Comparative study for the prediction of cavitating flow inside a square-edged orifice using different commercial CFD software. In *E3S Web of Conferences* (Vol. 128, p. 06003). EDP Sciences.

[14] Hromadka II, T. V., & Rao, P. (2019). Examination of Computational Precision versus Modeling Complexity for Open Channel Flow with Hydraulic Jump. *Journal of Water Resource and Protection*, *11*(10), 1233.

[15] Rojas-Solórzano, L.R.; Anna, B.; Bradeddine, S.L.; Amon, C.H. Modeling and Simulation of a Rollerball Microfluidic Device, ICNMM2009-82010. In Proceedings of the 7th International Conference on Nanochannels, Microchannels and Minichannels, Pohang, Korea, 22–24 June 2009.

[16] Islamov, M., Sypabekova, M., Kanayeva, D., & Rojas-Solórzano, L. (2017). CFD modeling of chamber filling in a micro-biosensor for protein detection. *Biosensors*, *7*(4), 45

[17] Zhang, B., Korolj, A., Lai, B. F. L., & Radisic, M. (2018). Advances in organ-on-a-chip engineering. *Nature Reviews Materials*, *3*(8), 257-278

[18] Kang, J. H., Kim, Y. C., & Park, J. K. (2008). Analysis of pressure-driven air bubble elimination in a microfluidic device. *Lab on a Chip*, *8*(1), 176-178.

[19] Kulsharova, G., & Kurmangaliyeva, A. (2021). Liver microphysiological platforms for drug metabolism applications. *Cell Proliferation*, *54*(9), e13099.

[20] Kulsharova, G., Kurmangaliyeva, A., Darbayeva, E., Rojas-Solórzano, L., & Toxeitova, G. (2021). Development of a Hybrid Polymer-Based Microfluidic Platform for Culturing Hepatocytes towards Liver-on-a-Chip Applications. *Polymers*, *13*(19), 3215.

[21] Allen JW, Bhatia SN. 2003. Formation of steady-state oxygen gradients in vitro: application to liver zonation. Biotechnol. Bioeng. 82:253–62

[22] Tilles AW, Baskaran H, Roy P, Yarmush ML, Toner M. 2001. Effects of oxygenation and flow on the viability and function of rat hepatocytes cocultured in a microchannel flat-plate bioreactor. Biotechnol. Bioeng. 73:379–89

[23] Ehrlich, A., Duche, D., Ouedraogo, G., & Nahmias, Y. (2019). Challenges and opportunities in the design of liver-on-chip microdevices. *Annual review of biomedical engineering*, *21*, 219-239.

[24] Coleman, W. B., & Presnell, S. C. (1996). Plasticity of the hepatocyte phenotype in vitro: Complex phenotypic transitions in proliferating hepatocyte cultures suggest bipotent differentiation capacity of mature hepatocytes. *Hepatology*, *24*(6), 1542-1546.

[25] Super, A. S. M. (2014). *Oxygen monitoring in a microfluidic culture device for stem cell bioprocess development* (Doctoral dissertation, UCL (University College London)).

[26] McLimans, W.F., Crouse, E.J., Tunnah, K.V., Moore, G.E., 1968. Kinetics of Gas Diffusion in Mammalian Cell Culture Systems .I. Experimental. Biotechnology and Bioengineering, 10, 725–740.

[27] Metzen, E., Wolff, M., Fandrey, J., Jelkmann, W., 1995. Pericellular pO2 and O2 consumption in monolayer cell cultures. Respiration Physiology, 100, 101–106.

[28] Tanaka, Y., Sato, K., Yamato, M., Okano, T., & Kitamori, T. (2006). Cell culture and life support system for microbioreactor and bioassay. *Journal of Chromatography A*, *1111*(2), 233-237.

[29] Mehta, G., Lee, J., Cha, W., Tung, Y.-C., Linderman, J.J., Takayama, S., 2009. Hard Top Soft Bottom Microfluidic Devices for Cell Culture and Chemical Analysis. Analytical Chemistry, 81, 3714–3722

[30] Korin, N., Bransky, A., Dinnar, U., Levenberg, S., 2007. A parametric study of human fibroblasts culture in a microchannel bioreactor. Lab on Chip, 7, 611–617.

[31] Du, X., Qu, F. S., Liang, H., Li, K., Bai, L. M., & Li, G. B. (2017). Control of submerged hollow fiber membrane fouling caused by fine particles in photocatalytic membrane reactors using bubbly flow: Shear stress and particle forces analysis. *Separation and Purification Technology*, *172*, 130-139.

[32] Rennert, K., Steinborn, S., Gröger, M., Ungerböck, B., Jank, A. M., Ehgartner, J., ... & Mosig, A. S. (2015). A microfluidically perfused three dimensional human liver model. *Biomaterials*, *71*, 119-131.

Goldstein, Y., Spitz, S., Turjeman, K., Selinger, F., Barenholz, Y., Ertl, P., ... & Bavli, D. (2021). Breaking the third wall: Implementing 3d-printing technics to expand the complexity and abilities of multi-organ-on-a-chip devices. *Micromachines*, *12*(6), 627.

[33] Lundholt, B. K., Scudder, K. M., & Pagliaro, L. (2003). A simple technique for reducing edge effect in cell-based assays. *Journal of biomolecular screening*, *8*(5), 566-570.

[34] Mazzei, D., Guzzardi, M. A., Giusti, S., & Ahluwalia, A. (2010). A low shear stress modular bioreactor for connected cell culture under high flow rates. *Biotechnology and bioengineering*, *106*(1), 127-137.

[35] Pedersen, J. M., Shim, Y. S., Hans, V., Phillips, M. B., Macdonald, J. M., Walker, G., ... & Yoon, M. (2016). Fluid dynamic modeling to support the development of flow-based hepatocyte culture systems for metabolism studies. *Frontiers in bioengineering and biotechnology*, *4*, 72.

[36] Goldstein, Y., Spitz, S., Turjeman, K., Selinger, F., Barenholz, Y., Ertl, P., ... & Bavli, D. (2021). Breaking the third wall: Implementing 3d-printing technics to expand the complexity and abilities of multi-organ-on-a-chip devices. *Micromachines*, *12*(6), 627.

[37] Delon, L. C., Guo, Z., Oszmiana, A., Chien, C. C., Gibson, R., Prestidge, C., & Thierry, B. (2019). A systematic investigation of the effect of the fluid shear stress on Caco-2 cells towards the optimization of epithelial organ-on-chip models. *Biomaterials*, *225*, 119521.

[38] [36] Sufiandi, S., Obara, H., Enosawa, S., Hsu, H. C., Matsuno, N., & Mizunuma, H. (2015). Improvement of infusion process in cell transplantation: effect of shear stress on hepatocyte viability under horizontal and vertical syringe orientation. *Cell Medicine*, *7*(2), 59-66.